Correlated electronic properties of some graphene nanoribbons: A DMRG study

V. M. L. Durga Prasad Goli,[1,*] Suryoday Prodhan,[1,†] Sumit Mazumdar,[2,3,‡] and S. Ramasesha[1,§]
[1]*Solid State and Structural Chemistry Unit, Indian Institute of Science, Bangalore 560012, India*
[2]*Department of Physics, University of Arizona, Tucson, Arizona 85721, USA*
[3]*College of Optical Sciences, University of Arizona, Tucson, Arizona 85721, USA*
(Received 11 January 2016; revised manuscript received 23 May 2016; published 18 July 2016)

The significant electron-electron interactions that characterize the π electrons of graphene nanoribbons (GNRs) necessitate going beyond one-electron tight-binding description. Existing theories of electron-electron interactions in GNRs take into account one electron–one hole interactions accurately but miss higher-order effects. We report highly accurate density matrix renormalization group (DMRG) calculations of the ground-state electronic structure, the relative energies of the lowest one-photon versus two-photon excitations, and the charge gaps in three narrow GNRs within the correlated Pariser-Parr-Pople model for π-conjugated systems. We have employed the symmetrized DMRG method to investigate the zigzag nanoribbon 3-ZGNR and two armchair nanoribbons 6-AGNR and 5-AGNR, respectively. We predict bulk magnetization of the ground state of 3-ZGNR, and a large spin gap in 6-AGNR in their respective thermodynamic limits. Nonzero charge gaps and semiconducting behavior, with moderate to large exciting binding energies, are found for all three nanoribbons, in contradiction to the prediction of tight-binding theory. The lowest two-photon gap in 3-ZGNR vanishes in the thermodynamic limit, while this gap is smaller than the one-photon gap in 5-AGNR. However, in 6-AGNR the one-photon gap is smaller than the two-photon gap and it is predicted to be fluorescent.

DOI: 10.1103/PhysRevB.94.035139

I. INTRODUCTION

Carbon has come to the fore in the past few decades for many exciting electronic and magnetic properties with the discovery of fullerenes in the 1980s to carbon nanotubes in the 1990s to graphene and graphene nanoribbons in the past decade [1–3]. In all these systems, we can assume that the carbon atom is in sp^2 hybridization and, hence, these systems belong to the class of π-conjugated carbon systems. In recent years, graphene nanoribbons (GNRs) have attracted considerable attention because of their exotic electronic properties and plausible applications in nanoelectronics [4–8]. GNRs with different widths can be made using various techniques like mechanical cutting of exfoliated graphenes or by patterning epitaxially grown graphenes [9–14]. GNRs are quasi-one-dimensional forms of graphene, which exhibit exciting electronic properties because of the confinement of electrons in low dimension [4,15–18]. These electronic properties also depend crucially on the geometry of the edges of the ribbons. The GNRs are classified into two types based on the edge structures, namely, zigzag and armchair GNRs (ZGNRs and AGNRs, respectively). Within the one-band tight-binding theory, ZGNRs are predicted to be metallic with zero band gap, while AGNRs can be either semiconducting or metallic, depending upon their width [15–17,19]; AGNRs with $3p + 2$ (with integer p) dimer bonds between nearest-neighbor carbon atoms across the ribbon width are metallic and others are semiconducting [17].

The quasi-one-dimensional character of the GNRs leads to confinement and enhanced electron repulsion between the π electrons. Thus extended screening lengths and long-range electron-electron interactions are expected in the semiconducting GNRs, and even in the metallic GNRs which are better described as zero-gap semiconductors [16,17]. Electron-electron interactions in GNRs and single-walled carbon nanotubes have been considered in the past within the time-dependent density functional approach [20–22] as well as the GW approximation accompanied by Bethe-Salpeter corrections [23–25]. These approaches take into account one electron–one hole ($1e$-1h) interactions, are equivalent to the single configuration interaction approximation of quantum chemistry [26–28], and have successfully predicted the excitonic character of the lowest optical absorption in the semiconductors. Our goal here, however, is to probe the consequences of the strong four-fermion two electron–two hole ($2e$-2h) interactions. As in previous work [26–28], we probe the consequences of realistic electron-electron interactions on the optical and charge gaps in three narrow GNRs, the ZGNR with three carbon-carbon bonds across its width (3-ZGNR), and AGNRs with six and five carbon-carbon bonds across their widths (6-AGNR and 5-AGNR), respectively (see Fig. 1). Beyond this, however, we also probe their ground-state magnetic character and the spin gap. We further determine the relative energy orderings of the lowest one- versus two-photon states in all three nanoribbons. In the past, the experimental demonstration that the lowest two-photon state occurs below the optical one-photon state in linear polyenes [29], in contradiction to the predictions of tight-binding and Hartree-Fock theories [29], provided the most convincing demonstration of the strong electron correlations in these systems. More recently, similar experimental results have also been obtained from nonlinear optical measurements of graphene nanofragments [30]. Accurate computational investigation of the relative energy orderings of one- and two-photon states also requires going beyond existing techniques. Finally, we compute nearest-neighbor bond orders (nearest-neighbor charge transfers) to examine the tendency to structural distortions.

*durgaprasad.vml@gmail.com
†suryodayp@sscu.iisc.ernet.in
‡sumit@physics.arizona.edu
§ramasesh@sscu.iisc.ernet.in

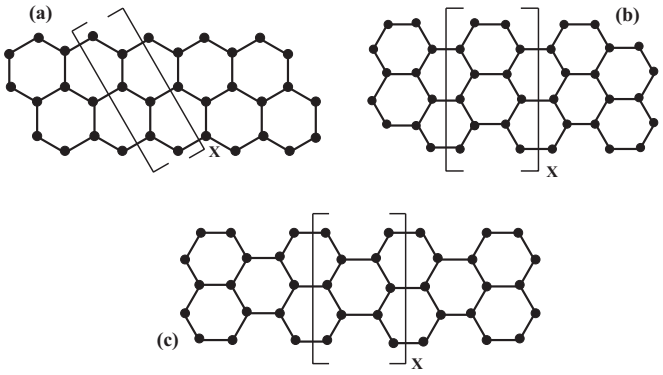

FIG. 1. Molecular structures of (a) 3-ZGNR, (b) 6-AGNR, and (c) 5-AGNR. The unit cell for each nanoribbon is indicated by the square brackets.

For conjugated carbon systems, the Pariser-Parr-Pople (PPP) model, which assumes $\sigma - \pi$ separability and incorporates long-range electron-electron repulsions [31], is known to reproduce ground and excited state properties very well [32–35]. It has also been demonstrated that the symmetrized density matrix renormalization group (DMRG) method can provide highly accurate descriptions of ground and low-lying excited states within the PPP model [36,37]. We report here symmetrized DMRG calculations on the three GNRs of Fig. 1.

We briefly mention here existing related works about edge magnetism in zigzag nanoribbons which was speculated quite early in the literature and has been studied rather extensively. Fujita *et al.* have studied both armchair and zigzag graphene ribbons with tight-binding approximation and reported the presence of a flat band and localized edge states near the Fermi level for zigzag nanoribbons, resulting in high density of states near the Fermi level [15]. In armchair nanoribbons, these almost flat bands (which are a consequence of the topology of the π conjugation) are absent. In the correlated picture, these almost flat bands result in magnetic states whose spins are arranged ferromagnetically at the edges [15]. Opposite edges of the ribbon will have opposite alignment of spins, making the ribbon nonmagnetic in the thermodynamic limit. Even in a general nanoribbon which cannot be classified as either perfectly armchair or perfectly zigzag, a few sequentially placed zigzag sites can result in a significant density of states at the Fermi level resulting edge ferromagnetism [16]. Sasaki and co-workers studied graphene in the continuous model using the Weyl equation with a special gauge field resulting from the local deformation in the π backbone and confirmed the presence of localized states at zigzag edges [38]. Consequences of the presence of these edge states in the quantum Hall effect in graphene have also been studied within localized [39] and continuum pictures [40]. Wakabayashi *et al.* studied electronic and magnetic properties of GNRs in the presence of a magnetic field in the tight-binding approximation and proposed that zigzag nanoribbons will show diamagnetic behavior at high temperature and paramagnetic behavior at low temperature [41]. Louie *et al.* have also showed that the edge-magnetic nature of ZGNRs can induce half metallicity in the presence of a transverse electric field across the ribbon width, resulting in a spin current [42]. The edge magnetism in zigzag nanoribbons has also been studied using the mean-field Hubbard model by Jung and co-workers [43], employing the quantum Monte Carlo technique by Golor *et al.* [44] and employing the renormalization technique by Hikihara *et al.* [45] and experimentally at room temperature by Magda and co-workers [46]. Instead of the presence of ferromagnetically aligned spins at the edges, all the above studies predicted a singlet ground state in ZGNR in the absence of an external field; however, a few density functional studies predicted a ferromagnetic ground state in ZGNR on doping [47]. Dutta *et al.* have studied low-energy properties of both zigzag and armchair GNRs within the Hubbard model using the quantum many-body configuration interaction method and predicted that the ground state of zigzag GNRs is a high-spin state, while for armchair GNRs the ground state is a singlet [48]. Spin-density calculations at the edges of zigzag nanoribbons show the presence of both up- and down-spin at a given edge instead of predominance of a specific spin as predicted by tight-binding and density functional theories. This study indicates that the picture can be significantly different in the presence of long-range electronic correlation.

There are also extensive studies of electronic properties such as band gaps and quasiparticle energies in GNRs. Ezawa has studied band gaps in a range of nanoribbons in the Hückel picture and predicted the width dependence of the band gaps in these systems [17]. He has also found that incorporation of edge effects by changing the transfer term or site energies of the edge sites has little effect on the band structure. Brey and Fertig studied the electronic structure of zigzag and armchair nanoribbons using the massless Dirac equation and their results are in agreement with the tight-binding results, except for narrow nanoribbons [19]. They proposed that the continuum analysis of graphene can quantitatively predict the properties of these nanoribbons. Louie *et al.* have computed the band gaps for zigzag and armchair GNRs by employing the first-principles approach within the local (spin) density approximation [49] and GW approximation with many-body Green's function technique [25] and proposed analytical expressions for band gaps as a function of GNR widths. They argued all GNRs to be semiconducting, contradicting earlier tight-binding predictions. Recently, spin and charge gaps of the armchair polyacene have been studied within the PPP model [50]. It has been shown that the ground state of armchair polyacene is a singlet and the system is an insulator in the ground state.

This paper is organized as follows. In Sec. II, we introduce the model Hamiltonian and briefly describe the DMRG scheme which we have employed in our study. In Sec. III, we present and discuss our results for the three GNRs. In the final section, we present a comparison of these three GNRs and summarize our results.

II. THEORETICAL MODEL, THE DMRG SCHEME FOR GNRS, AND SYMMETRY SUBSPACES

A. PPP Hamiltonian and parameters

The PPP Hamiltonian is written as

$$H = \sum_{\langle i,j\rangle,\sigma} t_{ij}(a^{\dagger}_{i\sigma}a_{j\sigma} + a^{\dagger}_{j\sigma}a_{i\sigma}) + \frac{1}{2}\sum_{i} U_i n_i(n_i - 1) + \sum_{i>j} V_{ij}(n_i - 1)(n_j - 1), \quad (1)$$

where $\langle i,j\rangle$ are the bonded pair of atoms and t_{ij} is the corresponding hopping or transfer integral, $a^{\dagger}_{i\sigma}$ ($a_{i\sigma}$) is the creation (annihilation) operator at site i with spin σ and n_i is the number operator. U is the Hubbard on-site repulsion and V_{ij} is the intersite electron-electron repulsion between carbon atoms i and j. V_{ij} are obtained from the Ohno parametrization [51],

$$V_{ij} = 14.397\left[\left(\frac{14.397}{U_i}\right)^2 + r_{ij}^2\right]^{-\frac{1}{2}}, \qquad (2)$$

which is arrived at by interpolating between U at $r_{ij} = 0$ and e^2/r_{ij} for $r_{ij} \to \infty$. In Eq. (2) the distances are in angstroms while the energies are in electron volts [52]. We have taken the nearest-neighbor distance between the carbon atoms as 1.42 Å and we fixed parameters $t_{ij} = -2.40$ eV and $U = 11.26$ eV as in many of the previous studies involving carbon-based conjugated systems [34,36,37]; the U value chosen [53] is the sum of the ionization energy and the electron affinity of carbon and gives the energy change in the process $CC \to C^+C^-$.

B. The DMRG scheme

We are interested in the properties of the three GNRs of Fig. 1 in the thermodynamic limit, which is reached from finite size scaling. Exact studies of the model Hamiltonian are confined, at best, to about 18 carbon sites and hence cannot be employed for extrapolation to the thermodynamic limit. Restricted configuration interaction approaches are not size consistent and cannot be employed with finite size scaling. The quantum Monte Carlo approach is also not suitable since we have long-range interactions in the model. For semiconducting narrow nanoribbons, the DMRG method is the method of choice as the area law of entanglement entropy holds and for the same DMRG cutoff similar accuracy is retained independent of the length of the nanoribbons [54,55]. In the case of metallic nanoribbons, gapless low-lying excitations are present and the area law of entanglement entropy will not hold. This leads to increasing errors with increasing system sizes in the DMRG method if we employ a fixed cutoff in the number of block states (M_l) for all system sizes. However, for finite systems in correlated models, there is always a finite gap in the excitation spectrum and, by keeping a large number of block states, we can deduce correct excitation energies. While our calculations do not reproduce all behaviors of metals, we believe that the particular properties we are investigating can be obtained from extrapolations of these excitation energies. It has also been shown that, for models with diagonal interactions in the real space such as the PPP model, the entanglement entropy is similar to those in the Hubbard and the Heisenberg models in one dimension [56]. Taken together, the above justify the use of the DMRG approach for PPP calculations of GNRs.

The DMRG method, discovered by White in 1992, divides a system block into two subblocks [54,55,57,58], generally referred to as the left subblock (L) and the right subblock (R), while the wave function of the total system block is described in the direct product space of these two subblock basis states. In the DMRG method, the Fock spaces of the two subblocks are approximated and it has been found that the best approximations of the subblock Fock spaces can be obtained by retaining a small number of reduced density matrix eigenvectors corresponding to the highest reduced density matrix eigenvalues. The reduced density matrix of a chosen subblock is obtained by treating the other block as an environment block and tracing the density over the states of the environment block. The reduced density matrix for a subblock of size l, so obtained, is diagonalized and M_l eigenvectors with the highest reduced density matrix eigenvalues are stored as column vectors of a $M_{l-1}d_\sigma \times M_l$ matrix where M_{l-1} is the number of density matrix eigenstates retained at the $(l-1)$th iteration and d_σ is the dimension of the Fock space of the new site added to the subblock at the lth iteration. The Hamiltonian of the subblocks is renormalized using this $M_{l-1}d_\sigma \times M_l$ matrix and the matrices of site operators are also transformed to this new basis. All terms in the PPP Hamiltonian including the long-range correlation terms can be expressed using these renormalized site operators, and the matrix elements of the system Hamiltonian can be obtained by taking appropriate direct products. The next step in the DMRG algorithm involves expanding the system block by adding a few sites (usually two) to the previous system block. The Hamiltonian matrix is constructed in the direct product basis of the retained block states of the two subblocks and Fock states of the newly added sites. From the Hamiltonian matrix, desired eigenstates are obtained and the process of constructing the reduced density matrix, truncating the Fock space of the augmented system, and expanding the system by adding two additional sites and again solving for the desired eigenstate is repeated until we achieve the targeted system size. The dimension of the Hamiltonian matrix is independent of the system size as the number of block states retained to span the Fock space of the subblocks is fixed, independent of the physical size of the subblock. The method described above is known as the infinite DMRG method.

In order to obtain the behavior in the thermodynamic limit using only the infinite DMRG method, we would need to retain a rather large number of block states (M_l) and go to much larger system sizes which is beyond our current computational capability. Instead, we have carried out finite DMRG calculations on systems of moderate sizes to obtain energy gaps with high accuracy and rely on finite size scaling to obtain the physical properties in the thermodynamic limit.

The finite DMRG algorithm was introduced by White to improve the accuracy of finite system calculations. In the infinite DMRG method, the density matrix of a p-site subblock is built from the eigenstates of a $2p$-site system block. This leads to errors in the target system of $2N$ sites ($N \gg p$). In order to correct this error, the p-site density

TABLE I. Exact versus DMRG ground-state energies (in eV) of 3-ZGNR, 6-AGNR, and 5-AGNR within the noninteracting model ($U = V_{ij} = 0$). The DMRG cutoff in the number of block states is 500.

System type and size	Ground-state energy	
	Exact calculation	DMRG method
3-ZGNR and 40 sites	−137.841	−137.738
6-AGNR and 40 sites	−139.503	−139.312
5-AGNR and 40 sites	−137.859	−137.813

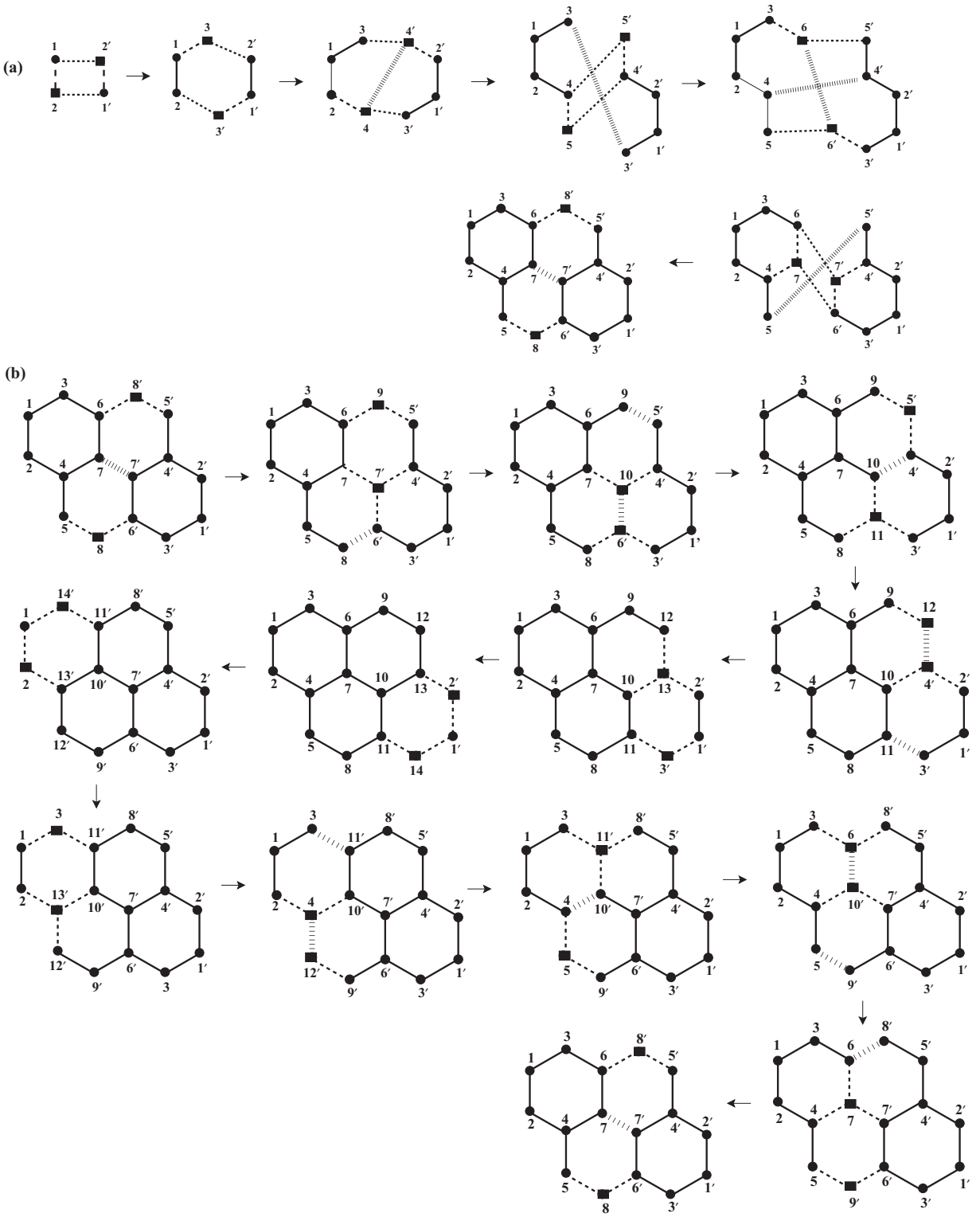

FIG. 2. (a) Construction of 3-ZGNR of 16 sites in the infinite DMRG method starting from a small system (four sites). The number of bonds between the new and the old sites at the intermediate system sizes are kept close to that in the final system for higher accuracy. At every step of the algorithm two new sites are added, one to the left subblock (L) and the other to the right subblock (R). The sites in L are denoted by numbers without primes while those in R are denoted by numbers with primes. The newly added sites are shown by solid squares (■) while old sites are denoted by solid circles (●). Solid lines are bonds within a subblock. The broken lines denote the bonds between ● and ■. Bonds between the two subblocks as well as the bonds between ■ are denoted by hatched lines. (b) Scheme for sweeping in finite DMRG method for 16-site ($2N = 16$) 3-ZGNR. In the forward sweep, the left block size increases from $N - 1$ to $2N - 2$ sites as the right block size decreases from $N - 1$ to 2 sites; in the reverse sweep, the opposite happens. During finite DMRG sweepings, the total system size remains constant. The corresponding figures for 6-AGNR and 5-AGNR are shown in Figs. 1–3 in the Supplemental Material [59].

matrices are iteratively constructed from the eigenstates of the $2N$-site target system block, until convergence is achieved. This procedure is termed "sweeping," where iteratively the size of one of the subblocks increases at the expense of the other, while the total system block size remains unchanged. At the final step of one full sweep, sizes of the two subblocks become equal and the same as in the infinite DMRG step. The finite DMRG procedure for molecular systems is nontrivial but essential as the energies improve considerably following the sweeping. We have employed the finite DMRG algorithm with a block state cutoff (M_l) of 500 and finite DMRG iteration of two sweeps to compare the DMRG method results with the exact calculation results for all three nanoribbons within the noninteracting model (Table I). The ground-state energies compare well with the exact nearest-neighbor tight-binding energies in all cases with a cutoff in the number of block states $M_l = 500$. For the interacting models, we expect the DMRG method to be more accurate for the same cutoff because interacting systems are less entangled. The method of constructing the GNRs in the infinite DMRG procedure as well as the method of finite sweeps are shown in Fig. 2 and Figs. 1–3 in the Supplemental Material [59].

C. Symmetry subspaces and one- versus two-photon excitations

The GNRs of interest possess C_2 symmetry along the axis perpendicular to the plane of the molecule, which we utilize in our computations as well as characterization of eigenstates. Eigenstates are labeled A or B depending upon whether they are of even or odd parity with respect to C_2 operation. The PPP Hamiltonian conserves total spin S, but total spin conservation is difficult within the DMRG scheme with large cutoff in the block states. We exploit partial spin symmetry by performing our calculations for the $S_z = 0$ sector in which the Hamiltonian has spin inversion symmetry, corresponding to invariance of the Hamiltonian when all spins of the system are reversed. This symmetry bifurcates the $S_z = 0$ space into a subspace with even total spin, i.e., $S = 0,2,4,\ldots$ (hereafter designated as "e") and another with odd total spin, $S = 1,3,5,\ldots$ (designated as "o"). Finally, the exactly half-filled band that we are investigating also exhibits charge-conjugation symmetry (CCS); eigenstates are labeled even or odd (hereafter + or −) depending upon the eigenvalue ± 1 reached when operated by the CCS operator [60,61]. The identity, the three symmetry operators, and their products form an Abelian group of eight elements. Hence, the $S_z = 0$ sector gets subdivided into eight subspaces.

In general, the ground state is even with respect to all symmetry operations and lies in the ${}^{e}A^{+}$ subspace. Optical one-photon states are reached by one application of the current operator j on the ground state,

$$\hat{j} = (i/\hbar) \sum_{\langle i,j\rangle,\sigma} t_{ij}(a^{\dagger}_{i\sigma}a_{j\sigma} - a^{\dagger}_{j\sigma}a_{i\sigma}), \tag{3}$$

which clearly changes the parity under C_2 symmetry while conserving S_z. It can also be shown that the application of the $\hat{j}$ changes CCS [60]. Two-photon states are reached by one application of $\hat{j}$ on the optical state (or two applications of the operator on the ground state), thus indicating that they also lie in ${}^{e}A^{+}$ subspace. In the $S_z = 1$ sector, spin inversion symmetry cannot be implemented and the lowest $S = 1$ state is in the B^{+} space. Using the symmetrized DMRG method [62] with a modified algorithm [63], all of these symmetries have been exploited in our calculations.

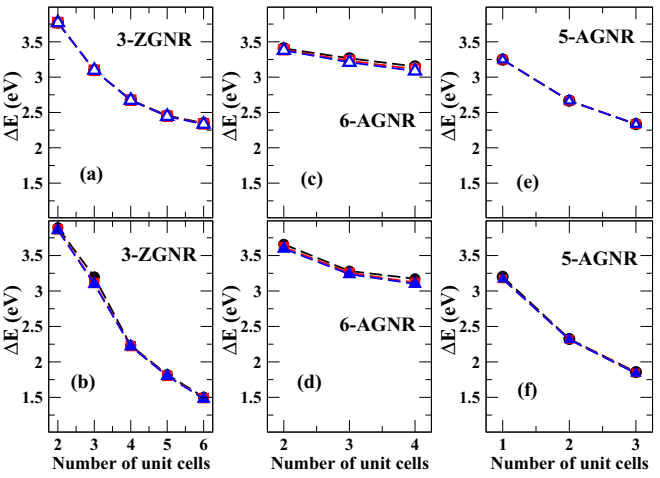

FIG. 3. Calculated lowest one-photon (optical) gaps (a, c, and e) and lowest two-photon gaps (b, d, and f) in short 3-ZGNR (left), 6-AGNR (middle), and 5-AGNR (right), plotted against the number of unit cells for different cutoff values of block states (M_l). The symbols denote the following: black open circle, one-photon gap with $M_l \simeq 750$; red open square, one-photon gap with $M_l \simeq 900$; and blue open triangle, one-photon gap with $M_l \simeq 1000$. Corresponding solid symbols denote two-photon gaps.

In each symmetry subspace, we have calculated a few low-lying energy states of the Hamiltonian using Davidson's algorithm for symmetric sparse matrices. At each step of the DMRG algorithm, block states are computed from the average reduced density matrix obtained from these eigenstates instead of the reduced density matrix of a single state. The average reduced density matrix is defined by $\rho = \sum_k \omega_k \rho_k$ where ρ_k are the reduced density matrices corresponding to eigenstates $|k\rangle$ and ω_k are the weights of the corresponding eigenstates [57]. We have taken $\omega_k = 1/N_k$, where N_k is the number of low-lying eigenstates computed in the symmetry subspace. In what follows we define all energy gaps with respect to the ground-state energy (thus the lowest one- and two-photon gaps are the energy differences between the corresponding eigenstates and the ground state).

In order to arrive at the desired cutoff in block states M_l for our calculations, we have calculated the lowest two-photon gaps and lowest optical gaps with different cutoffs for small systems of 3-ZGNR, 6-AGNR, and 5-AGNR (Fig. 3). We note that $M_l \simeq 750$ is adequate for comparisons with experiments in all three GNRs.

III. RESULTS AND DISCUSSION

We have used the unsymmetrized DMRG technique to calculate the ground-state energies of these nanoribbons within the PPP model (Fig. 4). The excellent linear fit of the energies as a function of system size shows that the procedure is stable and accurate.

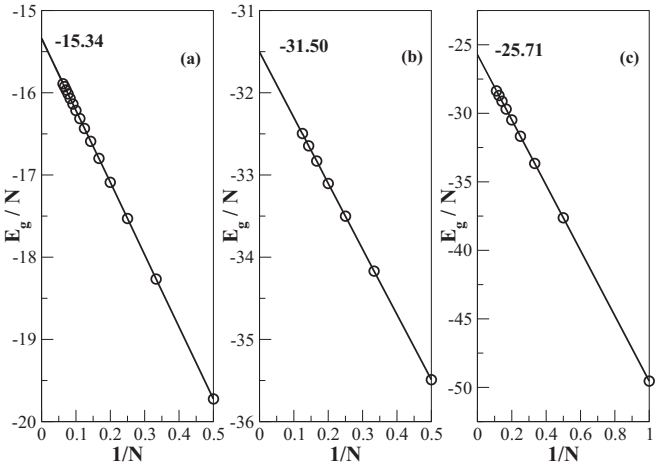

FIG. 4. Ground state energy in eV per unit cell versus $1/N$ for (a) 3-ZGNR, (b) 6-AGNR, and (c) 5-AGNR within the PPP model. Here N is the number of unit cells as depicted in Fig. 1.

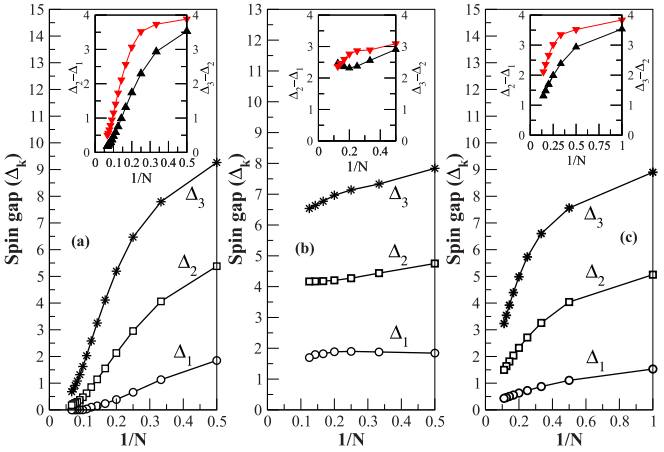

FIG. 5. Spin gaps (see text) in eV versus the inverse of the number of unit cells for (a) 3-ZGNR, (b) 6-AGNR, and (c) 5-AGNR within the PPP model. Insets: $\Delta_2 - \Delta_1$ (black solid up triangle) and $\Delta_3 - \Delta_2$ (red solid down triangle), also versus the inverse of the number of unit cells.

A. Spin gaps

As mentioned above, it is difficult to exploit total S invariance in the DMRG scheme. We have therefore computed the lowest energy states in the different S_z sectors; the total S are determined from the calculated energy gaps $\Delta_k = E_0(S_z = k) - E_0(S_z = 0)$, where $E_0(S_z = k)$ is the lowest energy in the $S_z = k$ sector. In the absence of an external magnetic field, the different z components of a given total S are degenerate; thus $\Delta_1 = 0$ implies that the ground state lies in the total spin $S = 1$ subspace. This is true for arbitrary Δ_p, and hence in general for $\Delta_1 = \Delta_2 = \cdots = \Delta_p = 0$ and $\Delta_{p+1} > 0$, the ground state has spin $S = p$.

We have shown the dependence of the computed energy gaps (Δ_k) on the DMRG cutoff for a moderate-sized 3-ZGNR system in Table II. We find that keeping ∼750 block states is sufficient for getting accurate gaps. Among all GNRs in this study, the energy gaps are smallest in 3-ZGNR; hence, we expect the same cutoff to be adequate for AGNRs also.

In Fig. 5(a) we have plotted spin gaps Δ_k as a function of the inverse of the number of unit cells (N) for 3-ZGNR. For $N < 14$, we find $\Delta_1 > 0$, indicating that the ground state is a singlet. For $N \geqslant 14$, $S_z = 1$ and $S_z = 0$ states are degenerate (within the DMRG accuracy), which implies that the ground state has $S = 1$. $\Delta_2 > 0$ in this region, but becomes smaller as N is further increased. It appears that $S = 2$ will become the spin of the ground state for larger N values. Similarly, the gap between $S_z = 3$ and $S_z = 0$ states also decreases with increasing N. The inset in Fig. 5(a) shows the behavior of $\Delta_3 - \Delta_2$ and $\Delta_2 - \Delta_1$, both of which rapidly approach zero at large N. From these trends in the the spin gaps, we predict that the ground state of this system is ferromagnetic in the thermodynamic limit.

TABLE II. Different Δ_k values in eV calculated for 3-ZGNR with five unit cells, for different numbers of retained block states. The changes in the energy gaps for the different cutoff values are not significant.

Block states cutoff	Δ_1	Δ_2	Δ_3
700	0.290	1.608	4.174
750	0.292	1.610	4.177
800	0.293	1.612	4.180

The spin gaps Δ_k for 6-AGNR are shown in Fig. 5(b). Δ_1 now exhibits weak size dependence and continues to be nonzero even in the thermodynamic limit. The extrapolated Δ_1 in the thermodynamic limit is 1.43 eV, which is actually larger than the noninteracting tight-binding band gap of 1.19 eV. This implies that the ground state of this system is a singlet. Indeed Δ_1 is larger than that in polyacene which has a spin gap of ∼0.5 eV in the thermodynamic limit [37]. The spin gaps Δ_2 and Δ_3 are also large and weakly size dependent, as are the differences between the spin gaps $\Delta_2 - \Delta_1$ and $\Delta_3 - \Delta_2$, plotted in the inset of Fig. 5(b). In general $E(S) > E(S')$ for $S > S'$ here, where $E(S)$ is the lowest energy in the total spin S subspace, and the corresponding energy differences are large.

For 5-AGNR, the spin gaps between different S_z sectors and $S_z = 0$ are shown in Fig. 5(c). The extrapolated Δ_1 in the thermodynamic limit is 0.15 eV, indicating that the ground state is spin singlet. From the N-dependent behavior of Δ_2 and Δ_3 (see in particular the inset) it is conceivable that the energy spectrum above Δ_1 may be gapless.

It is instructive to see what is to be expected for the spin gaps in the noninteracting limit. The energy levels of the frontier molecular orbitals of the three GNRs are shown in Fig. 6. We see that in 3-ZGNR, the energy gap between frontier orbitals approaches zero rapidly, implying that switching on exchange interaction will lead to a high-spin ground state. In 6-AGNR, the gap between bonding and antibonding frontier orbitals is finite for all system sizes. Introduction of electron-electron interaction will therefore not change the spin of the ground state and the ground state will always be a singlet. In 5-AGNR, the gap between the bonding and antibonding frontier orbitals progressively decreases but remains finite for large system sizes. The small band gap implies a small spin gap in the interacting picture.

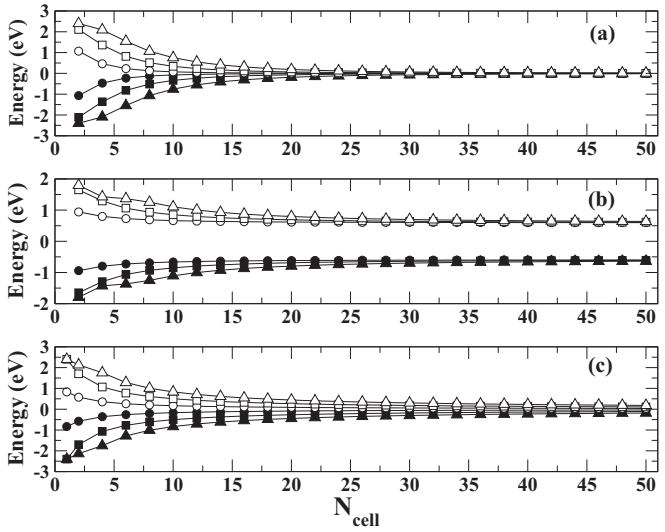

FIG. 6. A few energy levels near the Fermi level for (a) 3-ZGNR, (b) 6-AGNR, and (c) 5-AGNR within the tight-binding model are plotted as a function of the number of unit cells. The hopping energy considered is 2.40 eV. The symbol index is the same for all three panels and are as follows: solid circle, highest occupied molecular orbital (HOMO) energy level; solid square, HOMO-1 energy level; solid up triangle, HOMO-2 energy level; open circle, lowest unoccupied molecular orbital (LUMO) energy level; open square, LUMO+1 energy level; and open up triangle, LUMO+2 energy level.

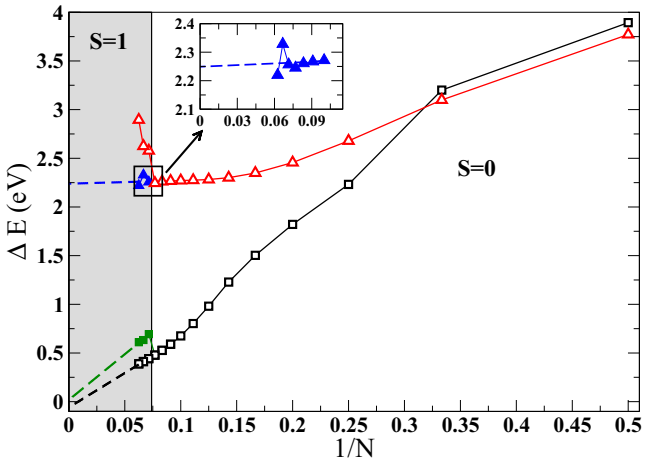

FIG. 7. Lowest optical and two-photon gaps in 3-ZGNR versus the inverse of number of unit cells. As the ground-state spin value changes on increasing the number of monomer units, the lowest optical gaps and lowest two-photon gaps in both $S = 0$ and $S = 1$ sectors are plotted. Symbols represent the following: △, lowest optical gap in singlet space; □, lowest two-photon gap in singlet space; ▲, lowest optical gap in triplet space; and ■, lowest two-photon gap in triplet space. Inset: Magnified plot of the lowest optical gaps and its extrapolation in 3-ZGNR systems, 11–16 monomer units.

In summary, the effects of electron-electron interactions on the three GNRs we have studied are very different and could not have been anticipated from their tight-binding electronic structures. The ferromagnetic ground state in 3-ZGNR is different from the edge-state ferromagnetism found earlier in wider ZGNRs [15,42,49]. More interestingly, while within tight-binding theory 5-ZGNR is metallic and is hence expected to be without a spin gap, we find a small but nonzero spin gap here, although the spectrum of spin excitations above the lowest gap may be gapless. As we show in Sec. III C, this system also has a nonzero exciton binding energy for nonzero electron-electron interactions. In 6-AGNR, which is a band semiconductor, both charge and spin gaps are expected within the tight-binding model. Our calculated results indicate that electron-electron interactions further enhance the spin gap here. We discuss these effects further in Sec. III B.

B. Excited-state ordering of one- versus two-photon states

As already mentioned in Sec. II C, the occurrence of the lowest two-photon states below the lowest optical one-photon states in linear polyenes [64,65] was the strongest evidence for higher-order Coulomb interaction effects beyond $1e$-1h interactions. It is therefore of interest to determine the excited-state ordering in these narrow GNRs we are probing; this is particularly so because, should the present systems become available experimentally, the corresponding two-photon states can be reached by a variety of nonlinear spectroscopic techniques, and our theoretical predictions tested.

We have obtained the low-lying one- and two-photon excited states for all three GNRs within the PPP model. We have done calculations starting from 2 units up to a maximum of 16 units of 3-ZGNR, from 2 units up to a maximum of 8 units of 6-AGNR, and from 1 unit up to 9 units of 5-AGNR, which correspond to about 100 carbon atoms in the largest systems studied. For extrapolation of different energy gaps in all three nanoribbons, we have considered the largest system sizes, specifically, from $N = 10$ to $N = 16$ for 3-ZGNR, from $N = 5$ to $N = 8$ in 6-AGNR, and from $N = 4$ to $N = 9$ in 5-AGNR (N is the number of unit cells).

In 3-ZGNR, the lowest two-photon state occurs above the lowest optical state for system sizes up to three units, but this energy ordering is reversed in larger systems (Fig. 7). Similar size dependence has also been observed in linear polyenes and is expected from theoretical considerations [29]. As pointed out above, the ground state of 3-ZGNR changes beyond a certain size. We have therefore plotted in Fig. 7 the lowest optical and two-photon gaps for both $S = 0$ and $S = 1$ ground states. In the Fig. 7 inset, the data points are shown on an expanded scale and appear to be scattered. However, the calculated standard deviation [66] for the linear fit is small (0.036 eV). The extrapolated value of the optical gap in the thermodynamic limit is found to be 2.25 eV, irrespective of the ground-state spin, which is in contradiction to the prediction of a metallic state for this nanoribbon within one-electron theory (see also Sec. I). Note that for system sizes where the ground state is a triplet, the singlet optical gap increases with system size. This is an artifact that is irrelevant for the real system with a magnetic ground state. As shown in the figure as well as in the inset, the triplet and singlet optical gaps lie on the same continuous curve if the data from the artificially large singlet gaps are ignored. However, the two-photon gaps in both singlet and triplet spaces extrapolate to zero in the thermodynamic limit. In linear polyenes, the lowest two-photon state is known to be a quantum-entangled state of two triplets with overall

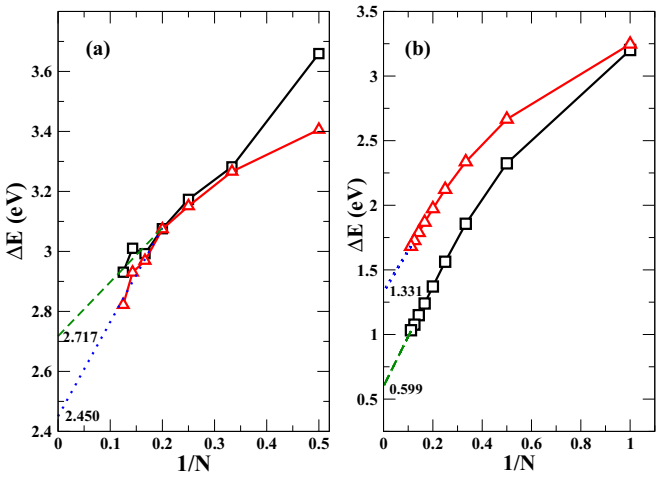

FIG. 8. Lowest one-photon (optical) (△) and two-photon (□) gaps in (a) 6-AGNR and (b) 5-AGNR, versus the inverse of the number of unit cells. The ground state remains in both cases in $S = 0$ space. The extrapolated one-photon and two-photon gaps are also indicated in the figures.

spin angular momentum of zero. The zero- gap two-photon state in the present case is to be anticipated, should the same theoretical description as a triplet-triplet state persist here.

In 6-AGNR, the lowest optical state always remains below the lowest two-photon state for all system sizes. The extrapolated one- and two-photon gaps at the thermodynamic limit are quite distinct [Fig. 8(a)]. The extrapolated value of the optical gap is 2.45 eV while that of the two-photon gap is 2.72 eV. The standard deviations of the linear fits of the optical gaps and the two-photon gaps are 0.032 and 0.026 eV, respectively. The larger two-photon gap here is a reflection of the predominantly band semiconductor character of 6-AGNR; therefore, the one-electron contribution to the optical gap must be larger than the many-electron contribution. The relative energy locations of the optical and two-photon states in 6-AGNR suggest that these systems will be fluorescent. In the case of 5-AGNR, on the other hand, the optical state always remains above the lowest two-photon state, although the lowest two-photon gap does not vanish in the thermodynamic limit [Fig. 8(b)] but saturates at a value of 0.60 eV. The optical gap in 5-AGNR extrapolates to 1.33 eV at the thermodynamic limit. An optical gap larger than the two-photon gap in 5-AGNR is a consequence of the former being dominated by Coulomb as opposed to band contribution.

C. Charge gap

We have calculated the charge gaps in these nanoribbons to explore the conducting nature in the thermodynamic limit, in the presence of long-range interactions (Fig. 9). The charge gap of a system with N unit cells, $\Delta_c(N)$, is defined as the energy required to create a well-separated electron-hole pair from the ground state of the system: $\Delta_c(N) = E^+(N) + E^-(N) - 2E^0(N)$, where $E^+(N)$ and $E^-(N)$ are the ground-state energies of the cation and anion, respectively, and $E^0(N)$ is the ground-state energy of the neutral system. In the thermodynamic limit, the charge gaps of 3-ZGNR,

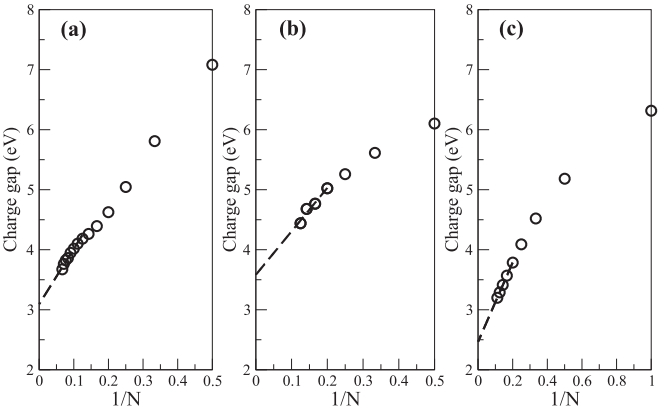

FIG. 9. Extrapolation of the charge gaps against the inverse of the number of unit cells, for (a) 3-ZGNR, (b) 6-AGNR, and (c) 5-AGNR, respectively.

6-AGNR, and 5-AGNR extrapolate to 3.09, 3.58, and 2.46 eV, respectively. Interestingly, the exciton binding energy (E_{xb}) of the optical state (E_{1ph}), which is measured as $E_{xb} = E_{cg} - E_{1ph}$, is quite small in all the three GNRs compared to other known organic conjugated systems. The exciton binding energies are 0.84 eV in 3-ZGNR, 1.13 eV in 6-AGNR, and 1.13 eV in 5-AGNR. Hence, these conjugated systems can have importance in molecular photovoltaics as the electron-hole pair can be relatively easily disassociated.

D. Bond order

We have calculated bond orders for the ground state and a few low-lying excited states of the largest systems we studied. The bond order (p_{ij}) for the $\langle i,j\rangle$ bond in a given state $|R\rangle$ is defined as $(-\frac{1}{2})\sum_\sigma \langle R|(a^\dagger_{i\sigma}a_{j\sigma} + \text{H.c.})|R\rangle$, and their deviation from an average value shows the tendency for the bond to distort. If the bond order is more (less) than the average, we expect the bond to shorten (lengthen) at equilibrium geometry. The numbering of bonds in the interior units of 3-ZGNR, 6-AGNR, and 5-AGNR are shown in Fig. 10. The bond orders towards the ends of the ribbons are normally different from the bond orders in the interior because of edge effects. In Table III, the bond orders of the interior unit of 3-ZGNR are given. In the 3-ZGNR series, we have given bond orders for two different system sizes: one with 13 monomer units, which has a singlet ground state, and another one with 16 monomer

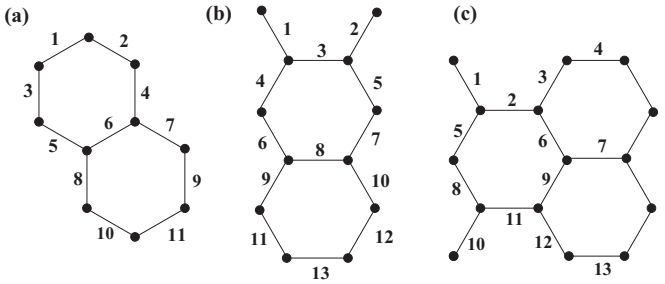

FIG. 10. Bond indices for the interior bonds of (a) 3-ZGNR, (b) 6-AGNR, and (c) 5-AGNR.

TABLE III. Bond orders of an interior unit of 3-ZGNR. Bond orders in systems with $\leqslant$13 monomer units are given in the first row while those for systems with $>$13 monomer units are given in the second row.

State	1	2	3	4	5	6	7	8	9	10	11
Ground state	0.54	0.56	0.47	0.47	0.52	0.52	0.52	0.47	0.47	0.56	0.54
	0.56	0.54	0.47	0.47	0.52	0.53	0.52	0.47	0.47	0.54	0.56
Optical state	0.54	0.57	0.46	0.46	0.54	0.50	0.54	0.46	0.46	0.57	0.54
	0.56	0.54	0.46	0.46	0.51	0.54	0.51	0.46	0.46	0.54	0.56
Two-photon state	0.52	0.58	0.48	0.47	0.50	0.54	0.50	0.47	0.48	0.58	0.52
	0.54	0.56	0.47	0.47	0.51	0.52	0.51	0.47	0.47	0.56	0.55
Spin state	0.56	0.53	0.47	0.47	0.52	0.53	0.52	0.47	0.47	0.53	0.57
	0.54	0.55	0.47	0.47	0.53	0.52	0.53	0.47	0.47	0.55	0.54

units with a triplet ground state. In both systems, the bond order differences between edge bonds in the ground state are small, implying almost uniform geometry of the edges. The rung bond orders are slightly smaller than the edge bonds, implying longer rung bonds than edge bonds at equilibrium geometry. The ground state, the optical state, and the lowest spin state all have similar geometries. The bond orders in the singlet and triplet two-photon states are similar away from middle of the ribbon. However, in the middle of the ribbon, the triplet two-photon state has marked single- and double-bond character in the top and bottom edge bonds (bonds 1, 2, 10, and 11).

The bond orders in 6-AGNR systems show somewhat different behavior (see Table IV). In the ground state, bonds on the ring and on the exterior of the edge (bond 13) show a tendency to contract, while bond 3 on the edge which is on the interior shows a tendency to expand. There appears to be a period (short-short-short-long) on one edge and out of phase by two bonds on the opposite edge. In the two-photon state, the bond orders remain almost the same as those in the ground state. In the one-photon state, there is considerable deviation in the bond orders in the central region of the nanoribbon, but the effect decreases towards the ends. However, in the triplet state it appears that this distortion is much more pronounced. Thus, the equilibrium geometries of the excited states are quite different from that in the ground state and we may expect larger Stokes shifts in the spectra of 6-AGNR compared to 3-ZGNR.

The bond orders on the edges of the 5-AGNR are similar to those in the 6-AGNR (see Table V). Except for the bonds which have rather large and small bond order values, all other bonds have nearly equal bond orders. So the distortion is expected more on the edges than in the interior. In all excited states, the interior bonds remain almost unperturbed. The edge bond structure in the central region of the nanoribbon shifts from short-long-short-short modulation to long-long-long-short modulation, while being unchanged towards the ends of the nanoribbon. The extent of distortion in the central region is highest in the two-photon and triplet states as compared to the one-photon state.

IV. CONCLUSION

We have studied correlated electronic properties of 3-ZGNR, 6-AGNR, and 5-AGNR within the PPP Hamiltonian with long-range Coulomb interactions. In all three cases the ground-state as well as excited-state behaviors are qualitatively different from the predictions of tight-binding theory, as summarized below.

We find 3-ZGNR to be a magnetic semiconductor with a Mott-Hubbard optical gap and a substantive exciton binding energy. The lowest two-photon state is gapless. The semiconducting behavior of 3-ZGNR is not entirely unanticipated, as similar Mott-Hubbard semiconducting behavior was previously predicted from correlated-electron calculations [67,68] and also experimentally demonstrated [69] in narrow single-walled carbon nanotubes which would be metallic within one-electron theory. As with 3-ZGNR, 5-AGNR is expected to exhibit metallic behavior within tight-binding theory, but it is also found to be a Mott-Hubbard semiconductor here, with now, however, a singlet ground state with small spin gap. The two-photon state is again below the optical gap. 5-AGNR thus resembles an idealized trans-polyacetylene strand, where bond dimerization leads to a spin gap, and where the occurrence of the two-photon state below the one-photon optical gap is believed to be a signature of greater Mott-Hubbard contribution to the optical gap than the contribution due to the Peierls bond dimerization [35]. In 6-AGNR, the one-electron optical gap is enhanced by Coulomb interactions, there occurs a large spin gap, and the two-photon state occurs above the optical gap. The overall behavior is reminiscent now of the conjugated polymers poly-paraphenylene and poly-paraphenylenevinylene, where the optical gap is dominated by the one-electron gap expected in systems with unit cells containing an even number

TABLE IV. Bond orders of an interior unit of 6-AGNR.

State	1	2	3	4	5	6	7	8	9	10	11	12	13
Ground state	0.58	0.59	0.37	0.57	0.56	0.44	0.45	0.51	0.57	0.56	0.58	0.58	0.66
Optical state	0.49	0.50	0.48	0.53	0.50	0.48	0.50	0.51	0.53	0.50	0.49	0.50	0.72
Two-photon state	0.57	0.57	0.38	0.54	0.54	0.47	0.47	0.50	0.55	0.54	0.56	0.58	0.65
Triplet state	0.48	0.48	0.50	0.52	0.48	0.48	0.51	0.51	0.52	0.48	0.47	0.48	0.73

TABLE V. Bond orders of an interior unit of 5-AGNR.

State	1	2	3	4	5	6	7	8	9	10	11	12	13
Ground state	0.60	0.39	0.60	0.63	0.51	0.51	0.52	0.51	0.51	0.61	0.39	0.60	0.63
Optical state	0.57	0.42	0.57	0.67	0.51	0.51	0.51	0.51	0.52	0.57	0.42	0.57	0.67
Two-photon state	0.50	0.48	0.51	0.72	0.52	0.52	0.49	0.52	0.52	0.51	0.48	0.50	0.71
Triplet state	0.52	0.47	0.51	0.72	0.52	0.52	0.50	0.52	0.52	0.52	0.47	0.51	0.72

of carbon atoms [33]. The three GNRs we have studied thus span the full range of behavior expected in quasi-one-dimensional correlated-electron systems. Conversely, the apparent similarities between these narrow GNRs and conjugated polymers reflect the deep and fundamental universality that exists among low-dimensional correlated-electron systems. Experimental tests of our theoretical predictions will provide fresh insight on the role of electron-electron interactions in carbon nanostructures. It is also of interest to determine how these features evolve upon controlled increase in the widths of GNRs. This is a topic of future research.

ACKNOWLEDGMENTS

We acknowledge the Indo-US Science and Technology Forum for financial assistance through a Joint Center, which made this collaboration possible. S.R. thanks DST for providing additional financial assistance. S.M. acknowledges partial support from National Science Foundation Grant No. DMR-1151475 and the UA-REN Faculty Exploratory Research Grant. S.P. acknowledges CSIR India for a senior research fellowship.

V.M.L.D.P.G. and S.P. contributed equally to this work.

[1] *Physical Properties of Carbon Nanotubes*, edited by R. Saito, G. Dresselhaus, and M. S. Dresselhaus (Imperial College Press, London, 1998).

[2] *Graphite Fibers and Filaments*, edited by M. S. Dresselhaus, G. Dresselhaus, K. Sugihara, I. L. Spain, and H. A. Goldberg (Springer-Verlag, Berlin, 1988).

[3] A. K. Geim and K. S. Novoselov, Nat. Mater. **6**, 183 (2007).

[4] A. H. C. Neto, F. Guinea, N. M. R. Peres, K. S. Novoselov, and A. K. Geim, Rev. Mod. Phys. **81**, 109 (2009).

[5] M. J. Allena, V. C. Tung, and R. B. Kaner, Chem. Rev. **110**, 132 (2010).

[6] S. Das Sarma, S. Adam, E. H. Hwang, and E. Rossi, Rev. Mod. Phys. **83**, 407 (2011).

[7] F. Schwierz, Nat. Nanotechnol. **5**, 487 (2010).

[8] *Graphene, Carbon Nanotubes, and Nanostructures: Techniques and Applications*, edited by J. E. Morris and K. Iniewski (CRC Press, Boca Raton, FL, 2013).

[9] C. Berger, Z. Song, X. Li, X. Wu, N. Brown, C. Naud, D. Mayou, T. Li, J. Hass, A. N. Marchenkov, E. H. Conrad, P. N. First, and W. A. de Heer, Science **312**, 1191 (2006).

[10] Z. Chen, Y.-M. Lin, M. J. Rooks, and P. Avouris, Physica E **40**, 228 (2007).

[11] M. Y. Han, B. Özyilmaz, Y. Zhang, and P. Kim, Phys. Rev. Lett. **98**, 206805 (2007).

[12] L. Tapasztó, G. Dobrik, P. Lambin, and L. P. Biró, Nat. Nanotechnol. **3**, 397 (2008).

[13] S. S. Datta, D. R. Strachan, S. M. Khamis, and A. T. C. Johnson, Nano Lett. **8**, 1912 (2008).

[14] X. Li, X. Wang, L. Zhang, S. Lee, and H. Dai, Science **319**, 1229 (2008).

[15] M. Fujita, K. Wakabayashi, K. Nakada, and K. Kusakabe, J. Phys. Soc. Jpn. **65**, 1920 (1996).

[16] K. Nakada, M. Fujita, G. Dresselhaus, and M. S. Dresselhaus, Phys. Rev. B **54**, 17954 (1996).

[17] M. Ezawa, Phys. Rev. B **73**, 045432 (2006).

[18] K. Wakabayashi and S. Dutta, Solid State Commun. **152**, 1420 (2012).

[19] L. Brey and H. A. Fertig, Phys. Rev. B **73**, 235411 (2006).

[20] A. G. Marinopoulos, L. Reining, A. Rubio, and N. Vast, Phys. Rev. Lett. **91**, 046402 (2003); A. G. Marinopoulos, L. Wirtz, A. Marini, V. Olevano, A. Rubio, and L. Reining, Appl. Phys. A **78**, 1157 (2004).

[21] H. Tachikawa, Y. Nagoya, and H. Kawabata, J. Chem. Theory Comput. **5**, 2101 (2009).

[22] B. F. Habenicht and O. V. Prezhdo, J. Phys. Chem. C **113**, 14067 (2009).

[23] C. D. Spataru, S. Ismail-Beigi, L. X. Benedict, and S. G. Louie, Phys. Rev. Lett. **92**, 077402 (2004).

[24] R. B. Capaz, C. D. Spataru, P. Tangney, M. L. Cohen, and S. G. Louie, Phys. Rev. Lett. **94**, 036801 (2005).

[25] L. Yang, C.-H. Park, Y.-W. Son, M. L. Cohen, and S. G. Louie, Phys. Rev. Lett. **99**, 186801 (2007).

[26] H. Zhao and S. Mazumdar, Phys. Rev. Lett. **93**, 157402 (2004).

[27] Z. Wang, H. Zhao, and S. Mazumdar, Phys. Rev. B **74**, 195406 (2006).

[28] Z. Wang, H. Zhao, and S. Mazumdar, Phys. Rev. B **76**, 115431 (2007).

[29] B. S. Hudson, B. E. Kohler, and K. Schulten, in *Excited States*, edited by E. C. Lim (Academic Press, New York, 1982), Vol. 6, p. 1.

[30] K. Aryanpour, A. Roberts, A. Sandhu, R. Rathore, A. Shukla, and S. Mazumdar, J. Phys. Chem. C **118**, 3331 (2014).

[31] R. Pariser and R. G. Parr, J. Chem. Phys. **21**, 466 (1953); J. A. Pople, Trans. Faraday Soc. **49**, 1375 (1953).

[32] P. Tavan and K. Schulten, J. Chem. Phys. **70**, 5407 (1979); **70**, 5414 (1979); **85**, 6602 (1986); Phys. Rev. B **36**, 4337 (1987).

[33] Z. G. Soos, S. Ramasesha, and D. S. Galvao, Phys. Rev. Lett. **71**, 1609 (1993).

[34] Z. G. Soos and S. Ramasesha, Phys. Rev. B **29**, 5410 (1984).

[35] D. Baeriswyl, D. K. Campbell, and S. Mazumdar, *Conjugated Conducting Polymers*, edited by H. Kiess, Springer Series in Solid-State Sciences Vol. 102 (Springer, Berlin, 1992).
[36] C. Raghu, Y. Anusooya Pati, and S. Ramasesha, Phys. Rev. B **65**, 155204 (2002); M. Kumar and S. Ramasesha, *ibid.* **81**, 035115 (2010); S. Thomas, Y. A. Pati, and S. Ramasesha, J. Phys. Chem. A **117**, 7804 (2013); S. Mukhopadhyay and S. Ramasesha, J. Chem. Phys. **131**, 074111 (2009).
[37] C. Raghu, Y. Anusooya Pati, and S. Ramasesha, Phys. Rev. B **66**, 035116 (2002).
[38] K. Sasaki, S. Murakami, and R. Saito, J. Phys. Soc. Jpn **75**, 074713 (2006).
[39] A. H. Castro Neto, F. Guinea, and N. M. R. Peres, Phys. Rev. B **73**, 205408 (2006).
[40] D. A. Abanin, P. A. Lee, and L. S. Levitov, Phys. Rev. Lett. **96**, 176803 (2006).
[41] K. Wakabayashi, M. Fujita, H. Ajiki, and M. Sigrist, Phys. Rev. B **59**, 8271 (1999).
[42] Y.-W. Son, M. L. Cohen, and S. G. Louie, Nature (London) **444**, 347 (2006).
[43] J. Jung and A. H. MacDonald, Phys. Rev. B **79**, 235433 (2009).
[44] M. Golor, T. C. Lang, and S. Wessel, Phys. Rev. B **87**, 155441 (2013).
[45] T. Hikihara, X. Hu, H.-H. Lin, and C.-Y. Mou, Phys. Rev. B **68**, 035432 (2003).
[46] G. Z. Magda, X. Jin, I. Hagymási, P. Vancsó, Z. Osváth, P. Nemes-Incze, C. Hwang, L. P. Biró, and L. Tapasztó, Nature (London) **514**, 608 (2014).
[47] S. Okada and A. Oshiyama, Phys. Rev. Lett. **87**, 146803 (2001); S. Dutta and S. K. Pati, J. Phys. Chem. B **112**, 1333 (2008).
[48] S. Dutta, S. Lakshmi, and S. K. Pati, Phys. Rev. B **77**, 073412 (2008).
[49] Y.-W. Son, M. L. Cohen, and S. G. Louie, Phys. Rev. Lett. **97**, 216803 (2006).
[50] M. Das, J. Chem. Phys. **140**, 124317 (2014).
[51] K. Ohno, Theor. Chim. Acta **2**, 219 (1964); G. Klopman, J. Am. Chem. Soc. **86**, 4550 (1964).
[52] A. Race, W. Barford, and R. J. Bursill, Phys. Rev. B **64**, 035208 (2001); **67**, 245202 (2003).
[53] L. Salem, *The Molecular Orbital Theory of Conjugated Systems* (W. A. Benjamin, Reading, MA, 1966), p. 420.
[54] U. Schollwöck, Rev. Mod. Phys. **77**, 259 (2005).
[55] K. A. Hallberg, Adv. Phys. **55**, 477 (2006).
[56] S. Sahoo, V. M. L. D. P. Goli, S. Ramasesha, and D. Sen, J. Phys.: Condens. Matter **24**, 115601 (2012).
[57] S. R. White, Phys. Rev. Lett. **69**, 2863 (1992); Phys. Rev. B **48**, 10345 (1993).
[58] S. Ramasesha, S. K. Pati, Z. Shuai, and J. L. Brédas, Adv. Quantum Chem. **38**, 121 (2000).
[59] See Supplemental Material at http://link.aps.org/supplemental/10.1103/PhysRevB.94.035139 for the method of constructing the AGNRs in the infinite DMRG procedure as well as the block-building scheme of finite sweeps for 6-AGNR and 5-AGNR.
[60] R. Pariser, J. Chem. Phys. **24**, 250 (1956).
[61] J. Cizek, J. Paldus, and I. Hubac, Int. J. Quantum Chem. **8**, 951 (1974).
[62] S. Ramasesha, S. K. Pati, H. R. Krishnamurthy, Z. Shuai, and J. L. Brédas, Phys. Rev. B **54**, 7598 (1996).
[63] S. Prodhan, S. Mazumdar, and S. Ramasesha, arXiv:1601.00053.
[64] B. S. Hudson and B. E. Kohler, Chem. Phys. Lett. **14**, 299 (1972).
[65] K. Schulten and M. Karplus, Chem. Phys. Lett. **14**, 305 (1972).
[66] S. C. Chapra and R. P. Canale, *Numerical Methods for Engineers*, 6th ed. (McGraw-Hill Education (India) Private Limited, New Delhi, 2012), Chap. 17 .
[67] Y. A. Krotov, D.-H. Lee, and S. G. Louie, Phys. Rev. Lett. **78**, 4245 (1997).
[68] L. Balents and M. P. A. Fisher, Phys. Rev. B **55**, R11973 (1997).
[69] V. V. Deshpande, B. Chandra, R. Caldwell, D. S. Novikov, J. Hone, and M. Bockrath, Science **323**, 106 (2009).